Macromolecules
ARTICLE

Macromolecules **2009**, *42*, 6261–6269 **6261**
DOI: 10.1021/ma9004346

Step Shear of Entangled Linear Polymer Melts: New Experimental Evidence for Elastic Yielding

Pouyan E. Boukany,[†,§] Shi-Qing Wang,*[,†] and Xiaorong Wang[‡]

[†]*Department of Polymer Science, University of Akron, Akron, Ohio 44325-3909, and* [‡]*Center for Research and Technology, Bridgestone Americas, Akron, Ohio 44317.* [§]*Present address: Department of Chemical Engineering, Ohio State University, Columbus, OH 43210.*

Received February 26, 2009; Revised Manuscript Received July 8, 2009

ABSTRACT: This work studies the most basic and important behavior of entangled linear polymer melts in sudden large shear deformations. In particular, melt elasticity resulting from the large step shear is extensively shown to produce cohesive breakdown. Unlike entangled solutions studied in *Macromolecules* **2007**, *40*, 8031, the residual elastic forces in sheared melts struggle quiescently for a significant induction period before bringing down the entanglement network. The induction time for the elastic yielding can be much longer than the longest Rouse relaxation time τ_R, making it difficult to associate this cohesive failure with a chain retraction process envisioned in the tube theory. The cohesive failure also occurs upon a step strain produced at rates too slow to produce chain stretching, again making it unreasonable to invoke the concept of chain retraction due to chain stretching.

I. Introduction

The field of polymer viscoelasticity and rheology is an integral part of polymer science and engineering and has a long and rich tradition. Today, the tube theory[1] based on the original Doi–Edwards (DE) theory[2,3] has been taken as the most successful molecular model for polymer entanglement dynamics. Its latest variant[4] contains corrections from contour length fluctuations, chain stretching, and convective constraint release. Any of its variants will be called the tube theory or tube model hereafter for simplicity. Although the original DE tube theory[2,3] has many shortcomings, one key extension[5] to predict nonlinear relaxation after large step shear strains has survived all the alternations[1,6] because it is in quantitative agreement with *some* experimental data.[7] In such a comparison, both experimental and theoretical studies regarded an entangled polymer to be capable of sustaining a great of deal of sudden strain without suffering mechanical failure either during or after straining. The impressive quantitative matching of the theoretical prediction of strain softening with step shear strain measurements (of amplitudes as high as 10 strain units) is widely known as the essential evidence that the tube model is even capable of depicting nonlinear viscoelastic processes. This consensus prevailed despite plenty of earlier experimental data[8−13] that deviated significantly from the quantitative description of the Doi calculation.[1,5]

What makes the comparison between the tube theory and experiment attractive is that both the experimental data and the theoretical calculation share one common characteristic: the shear stress after a large step strain would immediately undergo a sharp decline on a time scale t_b much shorter than terminal relaxation time τ before returning to normal relaxation that is approximately identical to the linear relaxation behavior. In the other words, the relaxation dynamics at times $> t_b$ seem universal, independent of the amplitude of the step strain, so that the data are superimposable by vertical shifting. This feature invited both experimentalists and theorists to characterize the stress relaxation behavior in the superimposable time domain ($t > t_b$) by introducing a time-independent damping function $h(\gamma)$, which is a normalized relaxation modulus equal to the ratio of the nonlinear "relaxation modulus" $\sigma(t,\gamma)/\gamma$ to the equilibrium relaxation modulus $\sigma(t,\gamma_0)/\gamma_0 = G(t)$, evaluated for $t > t_b$ and $\gamma_0 \ll 1$. The Doi calculation[5] recognized the stress decline to arise from chain retraction taking place on the Rouse relaxation time τ_R.

Unfortunately, the description based on h obscures one troubling feature of most experimental data including those that achieve quantitative agreement with the tube theory:[13,14] the declining shear stress at ($\tau \gg$) t' ($> t_b$) can be lower for an applied strain γ_2 than that for γ_1, i.e., $\sigma(t',\gamma_2) < \sigma(t',\gamma_1)$ for $\gamma_2 > \gamma_1$. In our judgment, unless the entanglement network is structurally altered, an entangled polymer cannot and should not have a lower residual shear stress for a higher applied strain. This characteristic has most often been concealed because literally all data were reported in the form of the damping function instead of the actual time-dependent shear stress that would have revealed the symptom.[13,14]

To reiterate, in our evaluation, the trend of decreasing $\sigma(t',\gamma)$ with increasing γ is not possible unless the network suffers structural failure during the step shear or after shear cessation. This judgment has led us to probing the step shear strain experiments with an effective particle tracking velocimetric (PTV) method.[13] The nonquiescent relaxation from a large step strain came as a huge surprise[14] because quiescent relaxation had always been perceived to occur according to the conventional wisdom including the tube theory.[1−5] This discovery of nonquiescent relaxation has led to a theoretical proposal[15] that (a) a finite cohesion can be defined for a well-entangled polymeric liquid on time scales much shorter than the quiescent terminal relaxation time and (b) elastic yielding is possible when a high step strain builds sufficient elastic retraction force to overcome the cohesion of the entanglement network. More importantly, it suggests that the constitutive theory based on the tube model was inadequate to depict macroscopic rheological phenomena including nonquiescent relaxation behavior after large step strain.

*Corresponding author. E-mail: swang@uakron.edu.

Published on Web 07/24/2009

Table 1. Microstructure Characteristics of SBR Melts

sample	M_w (g/mol)	M_w/M_n	% styrene	% butadiene	% vinyl (1,2-BD)	T_g (°C)
SBR(170K)	174 000	1.07	20	80	65.2	−22.7
SBR(250K)	250 000	1.04	20	80	65.0	−23
SBR(500K)	497 000	1.19	20	80	52.1	−35.4

Without having to perform a full continuum mechanical calculation, it is fair to question, in defense of the tube theory, whether the observed macroscopic motions after shear cessation could arise from chain retraction inside a tube upon a sudden step strain. In the tube theory, the chain contour length can exceed its equilibrium value during rapid straining, which is known as chain stretching, and chain retraction occurs if a step strain was produced at a rate faster than the Rouse relaxation rate $1/\tau_R$. Moreover, the chain retraction takes place on a time scale comparable to the Rouse relaxation time τ_R according to the tube theory.[1,5]

The present work explores the phenomenology involving step strain of a series of model polymer melts. By applying the particle-tracking velocimetric (PTV) method, we watch the aftermath of an interrupted rapid shear. The new phenomena pinpoint crucial elements that should be present in any new theoretical treatment. In particular, the cohesion of an entangled polymer is well-defined but can be overcome during relaxation after shear cessation. In this work, we found that the cohesive failure or the elastic yielding may occur over a time scale much longer than the characteristic Rouse relaxation time τ_R. Moreover, the cohesive failure was found to take place in absence of chain stretching for a step strain produced at a rate slower than the Rouse relaxation rate. This emerging phenomenology, observed in step-strained entangled melts for the first time, challenges the current theoretical framework that is based on the tube model and offers fresh insight into what new theoretical ingredients should be taken into account.

II. Experimental Section

A. Materials: SBR Synthesis and Characterization. Anionic polymerization of styrene−butadiene rubbers (SBR) of various molecular weights was conducted in hexane solution and in the presence of a modifier or a randomization controlling agent, so as to, for example, increase the reaction rate, equalize the reactivity ratio of monomers, and control the 1,2-microstructure in a conjugated diene. In this study, the modifier used was the oligomeric oxolanyl propanes (or OOPs). This chemical, when used in connecting with butyllithium (the initiator), can produce completely randomized SBR polymers in hexane. The detail regarding the preparation of oligomeric oxolanyl propanes and its application in rubber synthesis can be found elsewhere in United States Patent 4,429,090.

In preparation, butadiene in hexane (about 22 wt % butadiene), styrene in hexane (about 33 wt % styrene), pure hexane, and *n*-butyllithium in hexane (1.6 M in hexane) were used as supplied under nitrogen from the Firestone Synthetic. Neat oligomeric oxalanylpropanes (OOPs) obtained from the Firestone Polymer Co. were used as a 1.6 M solution in hexane, stored over calcium hydride. Other solvents such as isopropanol and the antioxidant butylated hydroxytoluene (BHT) were used as received. A 7.6 L reactor (Chemineer Inc.) equipped with a pitch blade impeller was used. The SBR polymers of this study were all made in this high-pressure closed reactor. The reactor was first charged with prescribed amounts of hexane, butadiene/hexane blend (22 wt % of butadiene), and styrene hexane blend. The batch was then heated to 57 °C. After the temperature stabilized, polymerization was initiated by adding a suitable amount of OOPs and then *n*-butyllithium in hexane. The batch temperature of 57 °C was maintained during the entire polymerization process. After about 5 h, the reaction was over, and the product was introduced into a solution of isopropanol and BHT and subsequently dried.

Table 2. Material Characteristics Based on Linear Viscoelastic Measurements at $T = 23$ °C

sample	M_w (g/mol)	M_w/M_n	M_e (g/mol)	G_N^0 (MPa)	τ (s)	τ_R (s)	$\tau_{R\eta}$ (s)
SBR170K	174 000	1.07	3300	0.67	120	2.3	1.9
SBR250K	250 000	1.04	3300	0.68	310	4.1	3.7
SBR500K	497 000	1.19	3100	0.72	2100	13	9.9

Molecular weights were determined by gel permeation chromatography (GPC) using Waters HSGPC equipment and tetrahydrofuran (THF) as solvent. Solid samples were weighed, dissolved in THF, and filtered before injection into the GPC column. The column was calibrated using polystyrene standards, and the averaged molecular weight of the sample was estimated based on these standards and a universal calibration curve.

The polymer microstructure such as vinyl and styrene content was determined by ^{1}H NMR measurements. A Varian Gemini 300 NMR spectrometer was used. The polymers were dissolved in a deuterated solvent ($CDCl_3$) and filtered before being transferred into a NMR tube for measurement. For all the polymers synthesized, NMR investigation on styrene absorption region revealed that there was no block styrene in existence. In other words, the amount of microblocks containing 2−8 consecutive styrene units is within 2%. The characteristic data of the SBR microstructures are listed in Table 1. Previous papers from our lab on uniaxial extension[16] and scaling characters of stress overshoot in startup shear[17] also investigated the same SBR samples.

A DSC 2910 differential scanning calorimeter was used to determine T_g of the SBR melts. The temperature at which the inflection point of heat capacity ($C_p = f(T)$) occurs was used as a measure of T_g. The temperature and the heat flow signals were calibrated with indium. The temperature scan rate was 10 °C/min.

B. Methods. *Linear Viscoelastic Measurements.* Small-amplitude oscillatory shear (SAOS, strain amplitude $\gamma = 5\%$) have been carried out to determine linear viscoelastic properties of these melts with an Advanced Rheometric Expansion System (ARES) using a parallel plate geometry with diameter of 15 mm and a gap of about 1 mm at room temperature ($T = 24$ °C). The actual data on storage and loss moduli G' and G'' have been published previously.[17] The molecular characteristics of these samples based on linear viscoelastic measurements are listed in Table 2, where the Rouse relaxation time is estimated in both ways, either as $\tau_R = \tau/(M_w/M_e)$, where the terminal relaxation time τ is the reciprocal of the crossover frequency at which storage and loss moduli equal to each other, or according to the zero-shear viscosity η using an approximate formula[18]

$$\tau_{R\eta} = (6M_w\eta/\pi^2\rho RT)(M_c/M_w)^{2.4}$$

PTV and Rheometric Measurements. A custom-built sliding-plate rheometer (SPR) with PTV capability was employed to measure rheological behavior and velocity profiles simultaneously. In our SPR, the bottom plate is fixed and upper plate is displaced by a step motor (Motion Parker Co., model ZETA6104-57-83). A load cell (Honey Well Co., model 13) was used to measure the rheological properties of the sample during shear and stress relaxation. The schematic depiction and details of our SPR with PTV setup has been described previously.[17,19] All the measurements were carried out at room temperature around 24 °C.

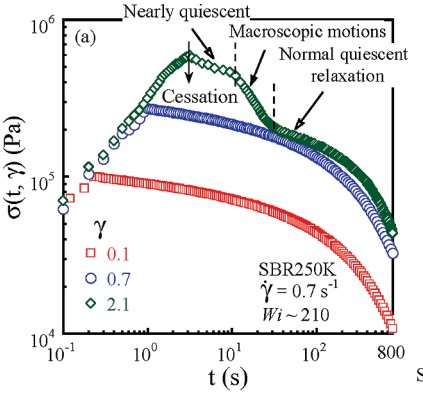

Figure 1a

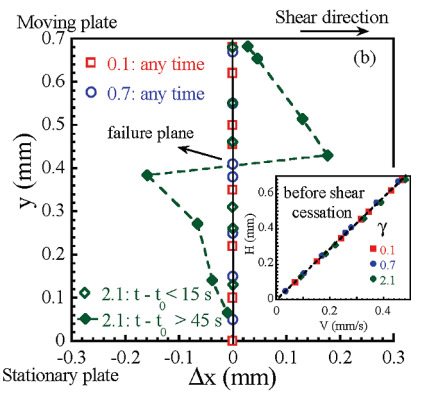

Figure 1b

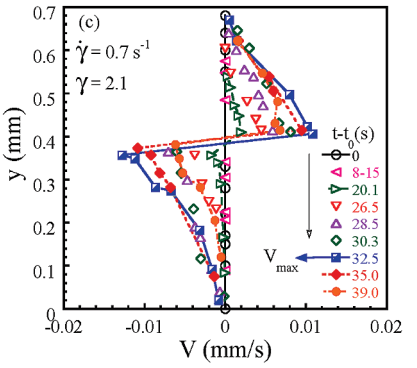

Figure 1c

Figure 1. (a) Shear stress growth and relaxation at three discrete strains of 0.1, 0.7, and 2.1 for SBR250K involving a shear rate of 0.7 s^{-1}. (b) PTV measurements of macroscopic displacements during relaxation, showing that no motions were measurable for $\gamma = 0.1$ and 0.7 at any time and for $\gamma = 2.1$ at any time before 15 s. After a 15 s induction time, considerable displacements of the tracked particles were observed to occur as shown by the filled diamonds, where the motions cease after $t - t_0 > 45$ s. The inset confirms homogeneous straining during the startup shear up to shear cessation. (c) After an induction period of 15 s, the quiescent sample started to display motions as revealed and measured by our PTV for $\gamma = 2.1$, where the maximum velocity was observed about 33 s after shear cessation.

For the purpose of PTV observations, SBR melts were first dissolved in toluene to achieve uniform solutions. Then around 600 ppm of silver-coated particles, averaged 10 μm in size, were dispersed uniformly in the solution. The toluene is subsequently removed first in the hood and then vacuum oven for several days. In the final step, bubble-free sheets of SBR melts were prepared with a CRAVER press. A sample of sufficient length L, width W, and thickness H, on the orders of $L \sim 30$ mm, $W \sim 10$ mm, and $H = 0.7-0.9$ mm, is first placed onto the sliding plate rheometer (SPR). A thin layer (around 10 μm in thickness) of commercial cyanoacrylate-based super glue (e.g., Instant Krazyglue) was used to attach the sample to the two plates so that wall slip does not occur during and after shear. In the absence of any such procedure, well-entangled polymer melts typically suffer massive wall slip,[19] making it impossible to carry out a proper step strain relaxation experiment. Because of the interfacial failure, ultra strain softening dominates the phenomenology.[20]

III. Results and Discussion

Since there are several sets of key experimental findings, the results will be presented in different subsections, each focusing on a different aspect of the remarkable behavior of sheared SBR melts. These results provide a possibility for explicit comparison with future full-scale continuum mechanical calculations based on various constitutive models including the widely used tube model.

A. Two-Stage Relaxation after Step Shear: Induction to Yielding. Step shear, i.e., an interrupted startup shear, has proved to be a most revealing experiment among all rheological tests of entangled polymers. At small amplitudes, such a test reveals finite cohesion in any well-entangled polymer on time scales much shorter than the terminal relaxation time τ. Our PTV observations indeed confirm that an entangled polymeric liquid remains intact upon a small step strain and exhibits linear relaxation behavior. Figure 1a shows that the stress relaxation behavior at amplitude $\gamma = 0.7$ is not different from that at $\gamma = 0.1$, demonstrating a finite level of cohesion that survives a 70% shear deformation. The stress relaxation behavior is very different for a step strain of $\gamma = 2.1$. There emerges two-stage behavior: First, the shear stress appears to relax in a similar way to that seen for $\gamma = 0.1$ and 0.7. Then sharp stress decline takes place, followed by normal relaxation behavior again. In other words, an induction time greater than 15 s passes before the sample shows a sign of deterioration in its ability to sustain the residual stress. Such behavior is in strong contrast to the stress relaxation behavior at high step strains of entangled solutions[13] where the stress decline occurs with negligible induction time after shear cessation.

Corresponding to the steep stress decline in Figure 1a, PTV observations capture what happens to the strained SBR melt. In contrast to the quiescent relaxation at lower strains of 0.1 and 0.7 depicted by the circles and squares in Figure 1b, for $\gamma = 2.1$ the sample appears to be intact in the first 15 s after shear cessation at t_0, judging from the insignificant motion across the gap. At $15 < t - t_0 < 50$ s, the tracked particles move in opposing direction in the

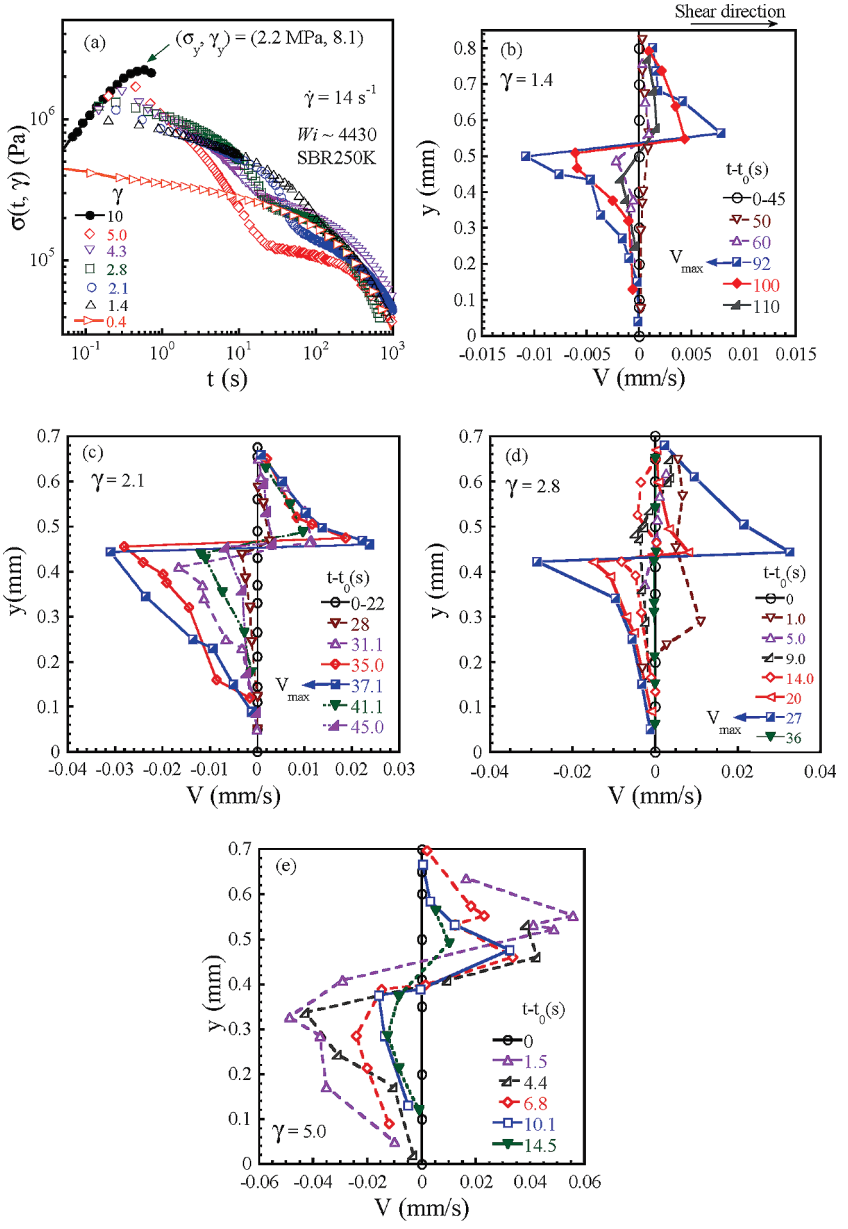

Figure 2. (a) Shear stress growth and relaxation at different strains ranging from 0.4 to 5.0 all before reaching the stress maximum for SBR250K involving a shear rate of 14 s^{-1}, where the full circles show appearance of the stress maximum σ_y at $\gamma_y \sim 8.2$. PTV measurements of macroscopic motions during relaxation are presented for (b) $\gamma = 1.4$, (c) $\gamma = 2.1$, (d) $\gamma = 2.8$, and (e) $\gamma = 5.0$.

sample interior as if a ductile rupture occurred. As the motions diminish after 45 s, the sample apparently "heals", and normal relaxation resumes as shown by the same stress relaxation as observed for small step strains. The inset of Figure 1b verifies that homogeneous deformation prevails up to the point of shear cessation, which is expected since all shear deformation has been found to be homogeneous in all of our PTV studies of solutions and melts before the shear stress overshoot and $\gamma = 2.1$ is significantly lower than the point of the stress maximum.

To further illustrate the "nucleation" of failure, we trace the evolution of the relaxing sample in terms of the velocity field at different times after shear cessation. Figure 1c shows that in the induction period of ca. 20 s there are only small motions. Maximum relative motions take place about 30 s after shear cessation.

This double-step relaxation is rather common for entangled melts in absence of wall slip. Figure 2a shows similar stress relaxation behavior to that in Figure 1a at a different shear rate of $\dot{\gamma} = 14\ s^{-1}$ at various strain amplitudes. The PTV measurements of nonquiescent relaxation are summarized in Figure 2b–e. Although the yield point at $\gamma_y = 8.2$ has not been reached, the system shows strong motions at $\gamma = 5.0$ with an induction time Δt_{ind} shorter than a second. It is important to note that the location of the fault plane is not fixed from one sample loading to another. In other words, there are cases when the breakup occurs near the sample/wall interface although there is no difference in the stress relaxation behavior. In this paper, we only present the cases where the failure took place in the sample interior to avoid any difficulty in the interpretation of such cohesive failure. Even when the failure is observed at the interface, often it is not due to an irreversible failure of the super glue since the sample heals over time and is able to again sustain high strain upon healing.

The induction time, at which motions are first measurable, Δt_{ind}, is seen to shrink with increasing strain amplitude γ. The data could fit a relationship for this "activation" time

that scales with γ in an Arrhenius way as shown in Figure 3: $\Delta t_{ind} \sim \exp(-\Delta G/k_BT)$ with $\Delta G = \gamma k_BT$.[15] The higher strain generates a higher level of elastic restoring energy, making it more rapid to overcome the quiescent cohesion (of the order k_BT per entangling strand). We interpret the emergence of macroscopic motions upon shear cessation at large strains as evidence of cohesive failure caused by the elastic retraction forces. This elastic yielding process has been theoretically discussed previously.[15] The inset of Figure 3 reconfirms that sample experienced homogeneous deformation for all the tested strains up to $\gamma = 5.0$ during shear. Note that this relationship in Figure 3 only applies when the step strain exceeds a critical level to cause elastic yielding. Empirically, this critical shear strain is around 1.0, below which the sample does break up and there is no induction time to speak of. Currently, we do not have proper language to depict the crossover from the quiescent linear response behavior to elastic yielding observed to occur at high enough strains. It also remains unknown whether the exponential dependence of Δt_{ind} on γ is true for step strains produced at other rates of shear deformation.

B. Comparison with Theory: Elastic Yielding vs Chain Retraction. Our explanation for the two-step relaxation is that the entanglement network first proceeds to relax "normally" as if it has experienced a small step strain until its cohesion is overcome by the residual elastic forces, which we term *elastic yielding*. Subsequently, the normal relaxation resumes as the decohesion process ceases upon healing.

The tube model[4,5] and slip-link model[6] predict two-stage relaxation for large step strain as well. The sharp stress drop during the relaxation was perceived to be caused by chain retraction toward the equilibrium contour length. The Doi calculation shows the chain retraction to occur free of any entanglement constraint on a characteristic longest Rouse relaxation time τ_R, independent of the strain amplitude. Because the shear stress is directly proportional to the amount of chain stretching in the tube model, the chain retraction results in a sharp decline in the residual elastic force or the calculated shear stress. After the chain returns to its equilibrium length, the remaining stress due to chain orientation relaxes in the same way as for small step strains, i.e., dictated by the quiescent reptation dynamics, where the stress is relatively flat until the reptation time τ is approached. It is important to note that none of the previous theoretical accounts of step strain anticipated elastic yielding or any nonquiescent relaxation. Does the chain retraction in the tube model provide the proper physics for the observed nonquiescent relaxation phenomenon? In other words, is the observed structural failure caused by the single-chain retraction process? In absence of a full-scale molecular dynamics simulation, we could only compare the experimental observations with the basic features of chain retraction in the tube model. One thing appears clear: chain retraction in the tube model does not lead to displacement of the center of mass (CM) and thus would not envision any macroscopic motions, which would necessarily involve CM displacement.

Our data in Figure 2a indicate that the onset of rapid stress decline systematically shifts to longer times with decreasing amplitude of the imposed step strain. Correspondingly, measurable motions also show up after a longer induction time for a lower imposed strain as shown in Figure 2b−e. More importantly, at a step strain of $\gamma = 1.4$, the induction time Δt_{ind} is as long as 50 s as determined from Figure 2b. This time scale far exceeds the Rouse relaxation time estimated either as $\tau_{R\eta} = 3.7$ s or $\tau_R = 4.1$ s, as listed in Table 2. It

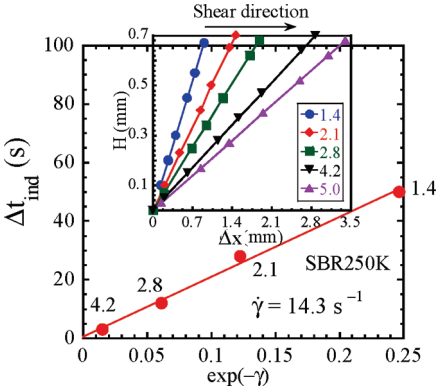

Figure 3. Induction time for yielding after various amplitudes of step strain γ produced at $\dot{\gamma} = 14\ s^{-1}$, Δt_{ind}, appears to change linearly with $\exp(-\gamma)$, where the four data points correspond to the strains of 1.4, 2.1, 2.8, and 4.2, respectively, as labeled. The inset shows that sample experiences uniform strain at the imposed strains from 1.4 to 5.0.

appears that the observed dynamics leading to failure are too slow to be associated with the chain retraction process prescribed by the tube theory.

Actually, it was clear to de Gennes ever since the first report[14] of nonquiescent relaxation in step-sheared entangled polymer solutions that the tube theory cannot offer an explanation. De Gennes had to propose an idea[21] that interfacial slip at the PTV particle surface initiates propagation of rupture-like failure. Since the phenomenon does not appear to depend on the PTV particle loading level, it was also suggested that the nonquiescent relaxation perhaps arises from the fracture of the free surface at the meniscus. Our unpublished data[22] have recently ruled out edge instability as the source of the observed failure.

Currently no detailed theoretical description is available to explain how the cohesive failure emerges in a heterogeneous manner after an induction period that ends in a steep stress decline and structural collapse. Because the yielding phenomenon is clearly a many-body process, some new nonequilibrium statistical mechanical approach is required to describe yielding. Beyond that, a separate "nucleation growth" theory for disentanglement is needed to explain why and how the molecular level process of elastic yielding (i.e., chains forced to pass by one another due to the internal elastic retraction forces) tends to occur in a heterogeneous fashion in well-entangled systems instead of homogeneous and uniform structural (topological) yielding.

C. Molecular Weight Effect. We have examined this elastic yielding behavior using two other SBR melts of different molecular weights so that the explored level of chain entanglement ranges from $Z = 53$ to 160 entanglement points per chain. A previous investigation[17] has revealed universal scaling behavior that at the same value of $\dot{\gamma}\tau_R$ (> 1) SBR melts of different molecular weights display identical responses up to the point of stress overshoot (or yield point). In light of the conclusions of that study, at a given value of $\dot{\gamma}\tau_R$, we can explore how the SBR melts relax upon the same amount of step strain well before the yield point.

Figure 4a shows that at $\dot{\gamma}\tau_R = 3$ the onset of stress decline is postponed as the number Z of entanglements per chain increases, where the inset show that the stress relaxation behavior is similar upon normalization of the time scale by τ_R. Figures 1c and 4b,c show the PTV analysis of macroscopic motions after shear cessation at the same strain for all three SBR melts with Z ranging from 53 to 160. According to our picture of elastic yielding upon step deformation,[15] the

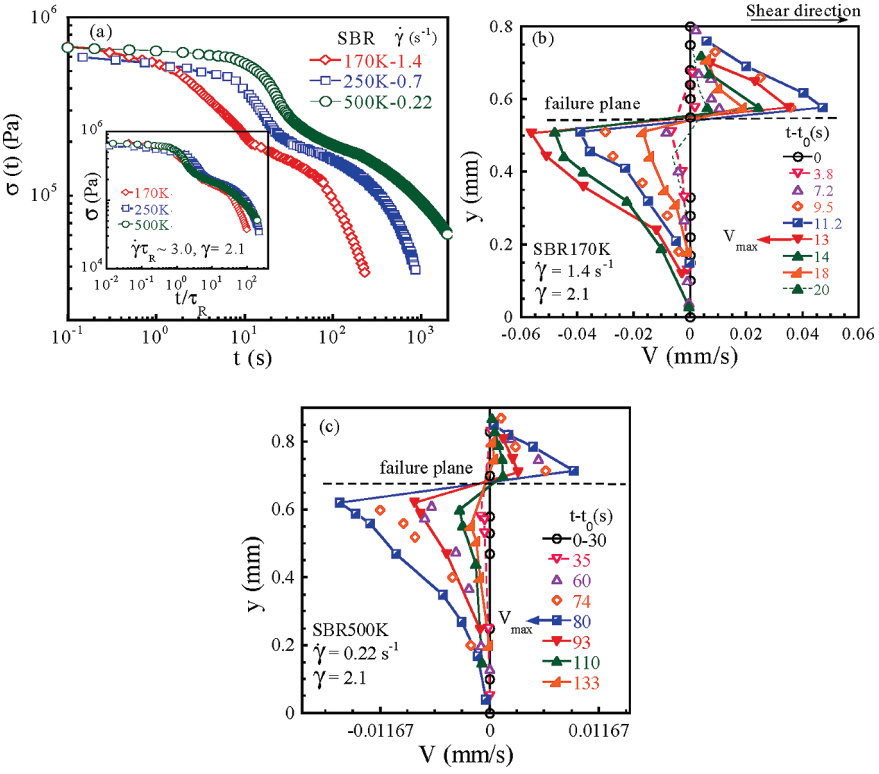

Figure 4. (a) Shear stress growth and relaxation of three SBR melts with different levels of entanglement with $Z = 53$, 76, and 160 involving a step strain of 2.1 where the Rouse−Weissenberg number $\dot{\gamma}\tau_R$ is around 3.0. The inset shows the stress relaxation of three SBR melts as a function of normalized time t/τ_R. PTV measurements of (b) SBR170K and (c) SBR500K during relaxation are presented.

driving force, i.e., the elastic retraction force, is the same for the three samples strained at the same normalized rate $\dot{\gamma}\tau_R \sim 3$, against the same level of cohesion.

By measuring the relative motions of the tracked particles as a function of time after shear cessation at t_0, corresponding to Figures 1c and 4b,c, we can conclude that the induction time Δt_{ind} approximately scales with τ_R as shown in Figure 5. In other words, the effect of molecular weight can be seen in terms of how Rouse chain dynamics dictate the kinetics leading to the eventual cohesive failure.

D. Step Strain at Different Rates: Significance of Yield Point. Along with the observations of universal scaling behavior at the yield point associated with startup shear of well-entangled melts,[17] emerged our picture of how yielding takes place during startup shear.[23] We have proposed that for well-entangled polymeric liquids the stress overshoot upon startup shear is a signature of yielding. Prior to the yield point at the stress maximum, the weaker-than-linear increase of shear stress with the apparent strain indicates that some load-bearing entanglement strands have disappeared. According to such a picture, the closer the system is brought to the shear stress maximum, the more load-bearing strands are lost. Before the stress maximum there may be a competition between further deformation in a load-bearing strand and loss of entanglement strands from chain ends. At a higher applied rate, the yield point occurs at a higher strain because the intermolecular gripping force increases with the deformation rate.[23]

In light of the preceding information and picture of yielding detailed elsewhere,[23] it would be interesting to examine the relaxation behavior from a step strain of the same amplitude that is generated at different shear rates. Figure 6a reveals a linear relationship, denoted by the dashed line, between the stress maximum σ_y and the yielding strain γ_y at σ_y, consistent with our previous report.[17] Step strain

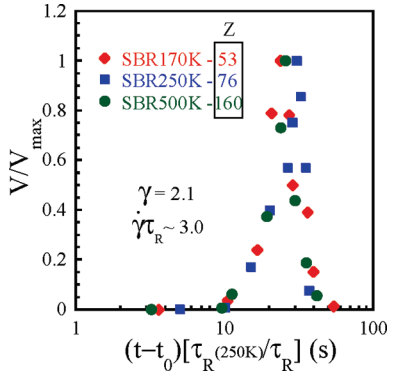

Figure 5. Normalized velocity V/V_{max} at the rupture planes for all three SBR melts as a function of the normalized time $(t - t_0)[\tau_R(250\ K)/\tau_R]$, revealing the significance of the Rouse relaxation time τ_R.

experiments have been carried out by interrupting these sudden startup shear experiments at a common elapsed strain of 2.1 as shown by the three open circles on the three curves. At $\dot{\gamma} = 14\ s^{-1}$, the point of shear cessation at $\gamma = 2.1$ is farthest from the yield point at $\gamma_y = 8.2$, but the residual shear stress is highest upon shear cessation. Applying any conventional reasoning, one would anticipate the relaxation to take place most rapidly for $\dot{\gamma} = 14\ s^{-1}$ and most slowly for $\dot{\gamma} = 0.7\ s^{-1}$. Intriguingly, the opposite is true as discussed below.

The rheological tests of step strain at these three rates to the same amplitude of $\gamma = 2.1$ is sufficiently revealing as shown in the inset of Figure 6b. Namely, the sharp stress decline occurs first for $\dot{\gamma} = 0.7\ s^{-1}$ despite the lowest shear stress level of the three. This result is significant in twofold. First, the trend of slower stress relaxation at a higher initial stress is remarkable. Second, no previous studies have ever

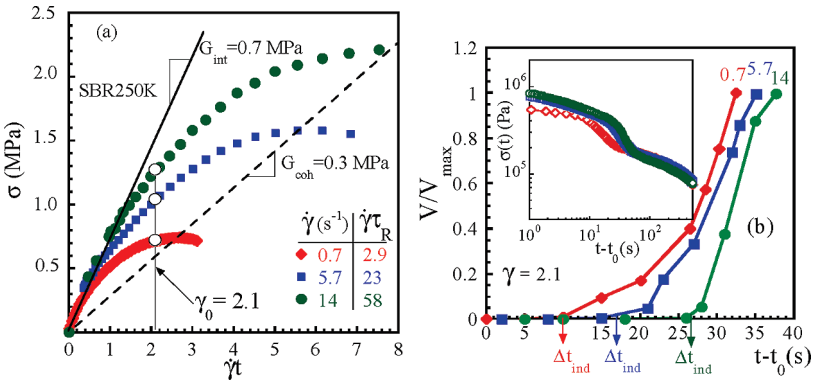

Figure 6. (a) Stress growth vs the elapsed strain $\dot{\gamma}t$ at $\dot{\gamma}$=0.7, 5.7, and 14 s^{-1} with $\dot{\gamma}\tau_R > 1$. (b) Normalized velocity V/V_{max} at the rupture planes after the step strain of 2.1 produced at $\dot{\gamma} = 0.7$, 5.7, and 14 s^{-1}. The inset shows the stress relaxation under the three different conditions.

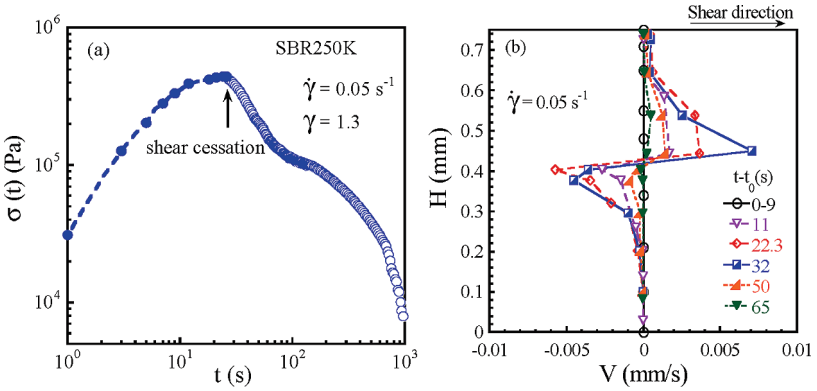

Figure 7. (a) Shear stress growth and relaxation for SBR250K at $\gamma = 1.3$ produced by a low shear rate of 0.05 s^{-1} corresponding to $\dot{\gamma}\tau_R \sim 0.21 < 1$. (b) PTV observations of the elastic yielding after shear cessation.

revealed this behavior, to our knowledge. These rheological experiments on entangled melts are challenging to do in a commercial rotational rheometer where the torque and normal force limitations are readily exceeded. More importantly, it is difficult to carry out PTV measurements from small fixtures that are required to avoid overloading the force transducers. The PTV results of Figure 6b show that at $\dot{\gamma} = 0.7$ s^{-1} strong macroscopic motions take place after the shortest induction time $\Delta t_{ind} \sim 10$ s, consistent with the stress relaxation behavior illustrated in the inset. This finding points to the significance of the stress overshoot: the closer the system is to the stress maximum, the more "damage" has already taken place. The higher stress associated with the higher rate perhaps only reflects a higher density of strands participating in the elastic deformation of the network rather than a higher level of molecular deformation.

E. Elastic Yielding after Step Strains at $\dot{\gamma}\tau_R < 1$. According to the tube model, a test chain does not extend beyond its equilibrium length by deformation that is produced at a shear rate below the Rouse relaxation rate $1/\tau_R$. In the absence of chain stretching, there is no chain retraction. In other words, for a step strain generated at $\dot{\gamma} < 1/\tau_R$, there should not be any fast relaxation mode, and the shear stress should only relax by chain reptation.

Figure 7a shows shear stress growth and relaxation where a startup shear at a rate of $\dot{\gamma} = 0.05$ s^{-1} is interrupted at a strain of $\gamma = 1.3$. This shear rate corresponds to Rouse–Weissenberg number $\dot{\gamma}\tau_R \sim 0.21$ or $\dot{\gamma}\tau_{R\eta} \sim 0.175$. In any variant of the tube model, the stress relaxation following such slow shearing is expected to take place on the time scale of the reptation, which is $\tau = 300$ s for this sample. Thus, the steep drop of the shear stress in Figure 7a on a time scale shorter than τ by a factor of 10 cannot be explained within the single-chain tube model. PTV observations reveal macroscopic motions as early as 11 s after shear cessation as shown in Figure 7b. This elastic yielding is clearly not attributable to any chain retraction, which is absent because of the condition of $\dot{\gamma}\tau_R < 1$. From our theoretical standpoint,[15] the elastic retraction force can still effectively build up as long as $\dot{\gamma}\tau > 1$. Thus, there can be sufficient residual elastic restoring force to overcome cohesion and caused chain disentanglement. In other words, the chains do not need to stretch beyond their equilibrium length to overcome the cohesion of the network. In contrast, for $\dot{\gamma}\tau_R < 1$ the tube model cannot contemplate any process leading to the observed failure in Figure 7b.

F. Yielding during Shear: Inevitable Fate of Entangled Liquids at High Rates. In this subsection, we examine startup simple shear carried out beyond the yield point or stress overshoot. Figure 8a shows the rheological responses of SBR250K during and after two respective strains of 7.14 and 5.0 at 1.4 and 0.7 s^{-1}, respectively. Figure 8b shows that the shear still remains uniform at $\gamma = 5.0$ at a shear rate of 0.7 s^{-1}, whereas at a shear rate of 1.4 s^{-1} the SBR melt has undergone shear banding at a strain of 6.7 before shear cessation. The PTV observations after shear strains of 5.0 and 7.14 are presented in parts c and d of Figure 8, respectively. Since the shear cessation occurred beyond the yield point, the type of macroscopic motions displayed in Figure 8c is vividly different from the sharp failure seen in Figures 1c, 2b–e, 4b,c, and 7b. Instead of experiencing sharp rupture-like failure, the state of the sample beyond the yield point is one where every layer is approaching the point of yielding. The breakdown after $\gamma = 5.0$ simply has to satisfy

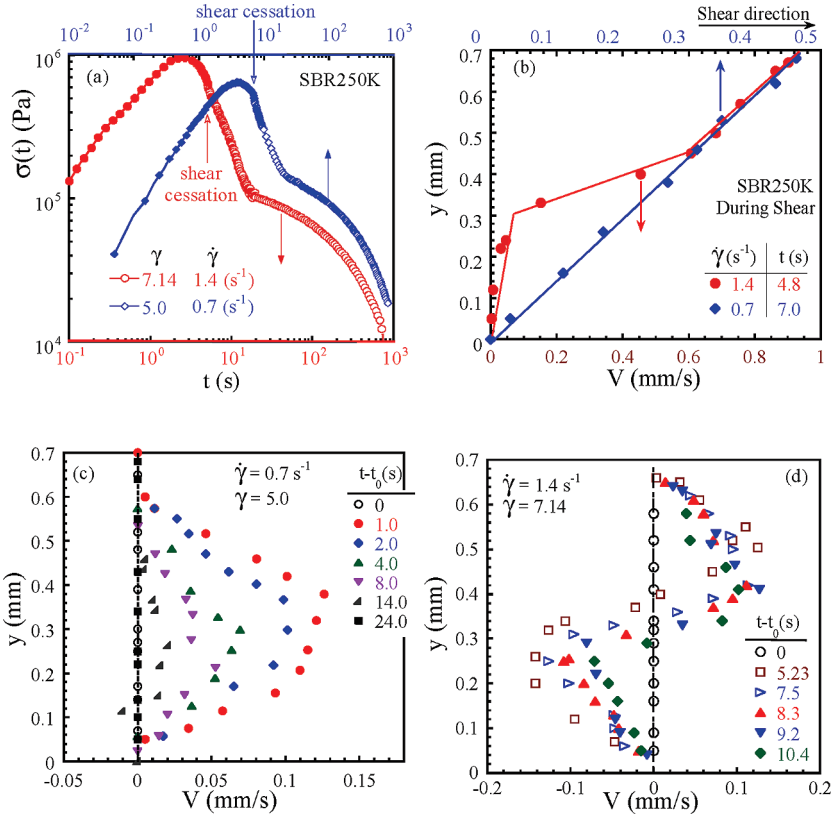

Figure 8. (a) Shear stress growth and relaxation for SBR250K $\gamma = 5.0$ and 7.1 produced at $\dot{\gamma} = 0.7$ and 1.4 s^{-1}, respectively. (b) PTV measurements during shear at $t = 4.8$ s (1.4 s^{-1}) and 7.0 s (0.7 s^{-1}). PTV measurements during relaxation at (c) $\gamma = 5.0$ and (d) $\gamma = 7.1$.

the no-slip boundary condition that allows maximum movements in the middle of the sample as shown in Figure 8c. In other words, in contrast to the behavior that involves step shear before the yield point, the breakdown of the entanglement network is much more homogeneous. The crack-like breakdown after $\gamma = 7.14$ in Figure 8d is, however, not surprising: a cohesive failure or shear banding has already occurred before shear cessation as shown in Figure 8b. Obviously, the system takes advantage of the existing structural weakness to relax its residual shear relaxation through recoil along the weakened layers.

IV. Conclusions

We have carried out a systematic investigation to explore characteristic relaxation behavior of several entangled linear SBR melts after step shear. The particle-tracking velocimetric observations allow us to correlate the shear stress responses with the state of macroscopic deformation. Among the most remarkable findings are: (a) There exists a significant quiescent (induction) period after shear cessation before a sheared sample eventually displays rupture-like cohesive failure in the form of concurrent macroscopic motions in opposite directions. (b) At low strains the system struggles quiescently for a period that is much longer than the longest Rouse relaxation time τ_R before elastic yielding produces measurable motions. (c) The induction time for elastic yielding shortens with increasing magnitude of the step strain. (d) The breakdown of the entangled melts occurs even when the step strain is produced at a rate slower than the Rouse relaxation rate. (e) For the same amplitude of step strain the induction time is actually longer when the step strain is produced at a higher rate despite a higher level of residual elastic stress that is available to work against the quiescent cohesion. All of these features are new and absent from previous PTV studies on polymer solutions. At this point, it appears difficult to for the tube theory to provide a proper description of the emerging phenomenology that has found some interpretations in our recently proposed theoretical picture[15,23] of entangled polymeric liquids undergoing large deformations. In particular, the nonquiescent relaxation observed after a step strain produced with a slower rate than the Rouse relaxation rate leaves us with no choice but to suggest the elastic yielding mechanism.

Acknowledgment. This work is supported, in part, by a grant (DMR-0821697) from Polymers program of the National Science Foundation.

References and Notes

(1) Doi, M.; Edwards, S. F. *The Theory of Polymer Dynamics*; Oxford University Press: Oxford, 1988.
(2) Doi, M.; Edwards, S. F. *J. Chem. Soc., Faraday Trans. 2* **1978**, *74*, 1789, 1802, 1818.
(3) Doi, M.; Edwards, S. F. *J. Chem. Soc., Faraday Trans. 2* **1979**, *75*, 32.
(4) Graham, R. S.; Likhtman, A. E.; McLeish, T. C. B.; Milner, S. T. *J. Rheol.* **2003**, *47*, 1171.
(5) Doi, M. *J. Polym. Sci.* **1980**, *18*, 1005.
(6) Doi, M.; Takemoto, J. *Philos. Trans. R. Soc. London* **2003**, *A361*, 641.
(7) Osaki, K.; Nishizawa, K.; Kurata, M. *Macromolecules* **1982**, *15*, 1068.
(8) Einaga, Y.; et al. *Polym. J.* **1971**, *2*, 550.
(9) Fukuda, M.; Osaki, K.; Kurata, M. *J. Polym. Sci., Polym. Phys.* **1975**, *13*, 1563.
(10) Osaki, K.; Kurata, M. *Macromolecules* **1980**, *13*, 671.
(11) Osaki, K. *Rheol. Acta* **1993**, *32*, 429.
(12) Venerus, D. C. *J. Rheol.* **2005**, *49*, 277.
(13) Ravindranath, S.; Wang, S. Q. *Macromolecules* **2007**, *40*, 8031.
(14) Wang, S. Q.; Ravindranath, S.; Boukany, P. E.; Olechnowicz, M.; Quirk, R. P.; Halasa, A.; Mays, J. *Phys. Rev. Lett.* **2006**, *97*, 187801.
(15) Wang, S. Q.; Ravindranath, S.; Wang, Y. Y.; Boukany, P. *J. Chem. Phys.* **2007**, *127*, 064903.
(16) Wang, Y. Y.; Wang, S. Q. *Phys. Rev. Lett.* **2007**, *99*, 237801.

(17) Boukany, P.; Wang, S. Q. *J. Rheol.* **2009**, *53*, 617.
(18) Osaki, K.; Inoue, T.; Uematsu, T.; Yamashita, Y. *J. Polym. Sci., Polym. Phys. Ed.* **2001**, *39*, 1704.
(19) Boukany, P.; Wang, S. Q. *Macromolecules* **2009**, *42*, 2222.
(20) Vrentas, C. M.; Graessley, W. W. *J. Rheol.* **1982**, *26*, 359.
(21) De Gennes, P. G. *Eur. Phys. J. E* **2007**, *23*, 3.
(22) Li, X.; Wang, S. Q. *J. Rheol.* **2009**, submitted.
(23) Wang, Y. Y.; Wang, S. Q. *J. Rheol.* **2009**, to be published.